

Synthesis, crystal structure, vibrational and optical properties of a new Pb(II) complex (2-hydroxyethyl)piperazine-1,4-dium tetrachloroplombate(II) $C_6H_{16}N_2OPbCl_4$

M. L. Mrad^{a,b*}, I. Feddaoui^a, Mohammed. S. M. Abdelbaky^c, S. García-Granda^c, C. Ben Nasr^a

^a*Université de Carthage, Laboratoire de Chimie des Matériaux, Faculté des Sciences de Bizerte, 7021 Jarzouna, Tunisie.*

^b*Université Tunis El Manar, Institut préparatoire aux études d'ingénieurs El manar tunis, Tunisie*

^c*Department of Physical and Analytical Chemistry, University of Oviedo-CINN, 33006 Oviedo, Spain.*

*Corresponding author: E-mail address: mraded@yahoo.fr

Abstract

A novel hybrid material, $C_6H_{16}N_2OPbCl_4$, has been successfully synthesized in nitrogen atmosphere by slow evaporation at room temperature. The compound structure was determined by single-crystal X-ray diffraction and crystallizes in the triclinic space group P-1 ($a = 5.9926(2)$ Å, $b = 10.3691(5)$ Å, $c = 11.3558(4)$ Å, $\alpha = 111.755(4)^\circ$, $\beta = 96.080(3)^\circ$, $\gamma = 105.948(4)^\circ$, $Z = 2$) at 293 K. The structure is built up from anionic 1-D polymeric chains of $PbCl_4O$ octahedral extended along the $(b + c)$ -axis. These chains are interconnected O-H...Cl hydrogen bonds to form inorganic layers parallel to $(a, b + c)$ plane. The organic layers are inserted between the inorganic ones and connect them through N-H...Cl and C-H...Cl hydrogen bonds to build a three dimensional network. To gain more information about intermolecular interaction we used Hirshfeld surfaces associated with 2D finger plots. The optical and PL properties of the compound were investigated in the solid state at room temperature and exhibited two bands at 250 and 290 nm and a photoluminescence emission at 529 nm. Raman and infrared spectra were used to gain more information for vibrational modes of the title compound. As for thermal analysis, DSC analysis shows that this compound is stable at temperature below melting point. Finally, XPS analysis is achieved for analyzing the surface chemistry of $C_6H_{16}N_2OPbCl_4$ crystals.

Keywords: Organic-inorganic hybrid; X-ray diffraction; Spectroscopy IR and Raman; Hirshfeld surface; Optic study; XPS and DSC.

1. Introduction

Hybrid materials offer important scientific and technological possibilities to combine attractive features of inorganic and organic systems within a single material [1-5]. This symbiosis between two worlds of chemistry too long regarded as antagonists can also lead to completely new properties, and opens up a vast field of investigation for the chemist. Inorganic materials offer high carrier density and mobility, high thermal stability and interesting magnetic or ferroelectric transitions, and organic materials offer great flexibility in the choice of molecules of length, width, polarizability and degree of saturation or polymerization. They also offer exceptional luminescent properties and potential for conductivity [6,7]. Hybrid materials based on metal halide units have attracted attention due to their interesting structural and optical properties, and their potential applications in light-emitting optical devices [8]. One of well investigated hybrid families is based on lead halides [9], in which organic ligands are inserted in the three dimensional inorganic parent structure to break it down to two, one or zero dimensions [10]. The lead (II)-based organic-inorganic layered materials have demonstrated enhanced exciton binding energies due to a dielectric confinement effect, nonlinear optical properties and electroluminescence [11,12]. In regards to the coordination geometries of elements of group 14 (limited to Sn(II) and Pb(II)) with halide atoms, the vast majority of cases are octahedra. Nevertheless, there are a lot of exceptions [13]. As for the organic ligands, we focused on 1-(2-hydroxyethyl) piperazine. Thus, piperazine and its derivatives are widely used due to their interesting biological and pharmacology proprieties. They are among the most important backbones in today's drug discovery industries. The piperazine scaffold is an important pharmacophore found in a large number of biologically active compounds [14-18]. Based on the above considerations, in the present work, we report the synthesis, structure, Hirshfeld surface, spectroscopic measurement, optical study and thermal analysis of a new hybrid material: (2-hydroxyethyl) piperazine-1,4-dium tetrachloroplombate(II), $C_6H_{16}N_2OPbCl_4$.

2. Experimental

2.1. Synthesis of $C_6H_{16}N_2OPbCl_4$

Crystals of $C_6H_{16}N_2OPbCl_4$ were prepared by dissolving in a concentrated solution of HCl (3 M, 10 mL) a stoichiometric mixture of $PbCl_2$ (1mmol, 0.278g) and N(2-hydroxyethyl)piperazine(1 mmol, 0.122 mL). The synthesis was produced in nitrogen atmosphere to prevent oxidation of Pb(II) to Pb(IV) [19]. Crystals suitable for X-ray analysis,

which remained stable under normal conditions of temperature and humidity, were isolated after several days by evaporating the resulting aqueous solution at room temperature (yield 72%). The chemical reaction scheme is:



2.2. Characterization

Single crystal X-ray structural analysis

A single crystal was carefully selected under a polarizing microscope in order to perform its structural analysis by X-ray diffraction. Diffraction data were collected on an Oxford Diffraction Xcalibur GeminiS diffractometer equipped with MoK α radiation (0.71073 Å). Intensities were corrected for Lorentz polarization and absorption effects [20]. The structure was solved by direct methods using SHELXL-97 [21] and refined against F² by full-matrix least-squares methods with anisotropic displacement parameters for all non-hydrogen atoms. All calculations were performed using SHELXL-97 implemented in the WINGX system of programs [22]. The drawings were made with the Diamond [23] and Mercury programs [24]. The refinement was done by full-matrix least squares methods (SHELXL-97 program) and converged to an acceptable final agreement factor.

The pertinent experimental details of the structure determination for the new compound are presented in Table 1. All hydrogen atoms were placed geometrically and refined isotropically.

The visualization and exploration of the intermolecular close contacts of the structure was achieved by calculating the Hirshfeld surface with the Crystal Explorer software [25]. All the bond lengths to hydrogen were automatically modeled to typical standard neutron values (C-H = 1.083 Å and N-H = 1.009 Å). In this study, the molecular Hirshfeld surfaces were generated using a standard (high) surface resolution with the 3D d_{norm} surfaces mapped over a fixed color scale from 0.42 Å (red) to 1.6 Å (blue). The 2-D finger print plots were displayed by using the standard range 0.6–2.6 Å.

Powder X-ray Diffraction

The powder X-ray diffraction (PXRD) was recorded on a Siemens D5000 powder diffractometer using Cu-K α radiation (1.542 Å) with a 2 θ range of 0–40°.

IR, Raman and UV measurements

The IR spectra were recorded in the 4000-500 cm⁻¹ range with a 1000 Perkin-Elmer FTIR spectrometer using samples dispersed in spectroscopically pure KBr pressed into a pellet.

The Raman spectrum was recorded between 50 and 2000 cm^{-1} at room temperature with a LABRAMHR 800 triple monochromatic instrument using a 514.5 nm line spectro-physics argon ion laser.

The UV absorption and optical diffuse reflectance spectra were measured at room temperature with a Perkin Elmer Lambda 11UV/Vis spectrophotometer in the 200-700 nm range.

Solid photoluminescence spectra were recorded using a time-resolved Edimburgh Instruments FLSP920 spectrofluorimeter with a Red-PMT detector and a Xenon bulb as an excitation source.

Calorimetric measurements

The differential scanning calorimetric (DSC) measurements were made on a SETARAM DSC131 ks instrument. A powder sample (11.7 mg) was heated from 273 K to 573 K with a ramp rate of 5 $\text{K}\cdot\text{min}^{-1}$ under a vacuum atmosphere.

XPS measurement

XPS spectra were recorded using a K-Alpha (Thermo) apparatus fitted with a monochromatic Al- $\text{K}\alpha$ X-ray source (spot size: 400 μm). The pass energy was set to 200 and 50 eV for the survey and the narrow regions, respectively. Electron and argon flood guns were used to compensate for the static charge build up of the powders. The composition was determined using the manufacturer's sensitivity factors.

3. Results and discussion

3.1 Powder X-Ray Diffraction Patterns

The powder X-ray diffraction (PXRD) experiments were recorded to confirm the phase purity of the material. The PXRD experimental and the simulated patterns based on a single-crystal structure are shown in Fig. 1. It perfectly matches the pattern simulated from the single-crystal diffraction data at room temperature, manifesting a pure phase of the bulky sample.

3.2 Description of the structure

The asymmetric unit of the title compound contains one PbCl_5 dianion coordinated to one monodentate organic ligands, 1-(2-hydroxyethyl) piperazine-1,4-diumdication (Fig. 2). The Cl(3) and Cl(4) reside on two-fold rotation axes. Each Pb(II) cation is coordinated by five chlorine atoms (Cl1, Cl2, Cl3, Cl4 and Cl5) and a ligand oxygen atom (O1) in a distorted

PbCl₅O octahedral geometry. The basic block of the C₆H₁₆N₂OPbCl₄ compound, as can be seen in Fig. S1, consists of adjacent PbCl₅O octahedra which are interconnected by chlorine bridges to generate an infinite 1-D coordination polymeric inorganic chain (PbCl₅O)_n running along the crystallographic (b+c) axis. In the atomic arrangement, the inorganic chains are interconnected via O–H···Cl hydrogen bonds to form an inorganic layer parallel to (a, b+c) plane (Fig. 3). The organic layers are inserted between the inorganic ones and connect them through N–H···Cl and C–H···Cl hydrogen bonds to form a three dimensional network (Fig. 4, Table 2). In the 1-D chains of Pb(II), three consecutive lead atoms Pb1', Pb and Pb'' are bonded via two bridge chlorides Cl3 and Cl4. The lead atom is connected to five chloride atoms with distances ranging from 2.721(2) Å to 3.0655(4) Å (Table S1). All the bond lengths and angles of the organic entity (Table S1) agree with those found in another salt containing the same cation, 4-hydroxy-1-methylpiperidinium [26]. The distances of the bridge chlorides Cl3 and Cl4 are 3.0655(4) Å and 2.8035(4) Å respectively. The Pb–O distance is 2.885 Å (Table S1). The Cl–Pb–Cl angles are varying from 79.91(5)° to 91.45(5)° for *cis* and 162.33(8)° to 169.078(12)° for *trans* arrangement. The equatorial trans angle for Cl–Pb–Cl is varied from 77.48(7)° to 91.45(5)°. Such a distortion from the ideal octahedral geometry is particularly attributed to the stereochemically activity of lead(II) lone pair electrons as previously reported [27]. The Pb–Cl–Pb angles equal to 180.00°, are close to those reported in the case of one-dimensional chain of slightly distorted octahedra [28]. The maximum deviation of the equatorial plane rms formed by PbCl₁Cl₂Cl₅O is -0.212 Å.

The conformation of the piperazine six-membered ring can be described in terms of Cremer and Pople puckering coordinates [29], i.e. evaluating the Q parameters (total puckering amplitude), q₂, q₃, θ and φ. Their calculated values for the N2–C3–C4–N1–C1–C2 ring are Q=0.5785Å, q₂=0.0072Å, q₃=-0.5784Å, θ =179.29° and φ =-164.35°, corresponding to the most stable chair conformation (Fig.S2). Its geometrical details are presented in Table S1, showing that the N–C, C–C and C–O distances are between 1.415(13) Å and 1.529(14) Å, and the N–C–C, C–N–C and C–C–O angles are varying from 108.7(8)° to 112.4 (8)°. This distances and angles agree well with those observed in other compounds with the same organic cation [14, 16].

3. 3 Hirshfeld surface

The Hirshfeld (HS) surface of the title compound was generated using CrystalExplorer 3.1 [25], which accepts a structure input file in CIF format. The HS is used to identify the intermolecular interactions including H···H, Pb···Cl, Cl···H and Cl···Cl contacts. The contacts with distances shorter than the sum of the van der Waals radii are indicated in red, the contacts with distances longer than Van der Waals radii are represented in blue, and the contacts with distances equal to the sum of van der Waals radii are indicated in white. The 3D d_{norm} surface can be resolved into 2D fingerprint plots, which analyze all intermolecular contacts at the same time and give a quantitatively summary of the nature and type of intermolecular contacts experienced by the molecules in the crystal.

The Hirshfeld d_{norm} surface, shape index and curvedness of the $\text{C}_6\text{H}_{16}\text{N}_2\text{OPbCl}_4$ are shown in Figure 5, and the 2D fingerprint plots showing the percentage of area occupied by the different types of intermolecular interactions are depicted in Fig. 6. The contributions from different interaction types which overlap in the full finger print are then separated (Fig. 6a).

The intensive red hot spots on the surface colored according to d_{norm} correspond to hydrogen bonds with neighboring molecules (N-H···Cl, O-H···Cl and C-H···Cl). The small, flat segments delineated by the blue outline in the surface mapped with curvedness indicate the absence of π ··· π stacking interactions in the structure. In addition, it is clear from the Hirshfeld surface that the crystal structure of $\text{C}_6\text{H}_{16}\text{N}_2\text{OPbCl}_4$ does not exhibit any π ··· π stacking interaction because there is no evidence of the adjacent red and blue triangles on the shape index surface. This result has been confirmed by X-ray crystal structural analysis.

The Hirshfeld surface analysis of the molecule shows that H···Cl and H···H interactions exhibit the most significant contributions (67.4 and 19 % of the total Hirshfeld surfaces, Figs. 6b and 6c, respectively). For the H···Cl interactions there are indeed five D-H···Cl hydrogen bonds in the crystal structure (Table2, Fig. 6b). The Pb···Cl intermolecular interactions appear as two short spikes in the 2D fingerprint plots, contributing to 5.7% (Fig. 6d). The 2D fingerprint plot reveals that the Pb···H interaction covers 4.1% of the total surface (Fig. 6e). Apart from the interactions mentioned above, the presence of Cl···Cl, O···H, Cl···O and Pb···O contact only contribute with 1.5% (Fig. 6f), 1% (Fig. 8g), 0.9% (Fig. 6h) and 0.3% (Fig. 6i) of the total Hirshfeld surfaces, respectively. This quantitative conclusion shows that the H···Cl interactions represent the important percentage of the total

surface and thus constitutes the driving force in the crystal packing (Fig. S3 contains the percentages of contributions for a variety of contacts in the title crystal structure).

3.4 Infrared Spectroscopy

The FTIR spectroscopy was used to identify the functional groups present in the crystal. The IR spectrum of $C_6H_{16}N_2OPbCl_4$ is shown in Fig. 7, was recorded for the wavenumbers region between 4000 and 500 cm^{-1} . The most representative and characteristic vibrational modes of this compound can be compared to those of similar materials [16, 30]. On investigating the spectrum, in the high-frequency region, between 3600 and 2300 cm^{-1} , the observed bands correspond to the stretching vibrations of the O-H, N-H and C-H. The hydrogen bonds interactions such as N-H...Cl, O-H...Cl and C-H...Cl (Table 2) affects the absorption positions in this region. The symmetrical CH_2 stretching frequency of the CH_2 group ($\nu_s(CH_2)$) next to nitrogen atom in secondary and tertiary amines, becomes intense and lower in frequency near 2800 cm^{-1} . So for N-(2-hydroxyethyl)piperazine-1,4-dium, the CH stretching bands appears at 3089, 2986, 2848 and 2770 cm^{-1} [16]. The bands at 1151 and 1117 cm^{-1} correspond to the asymmetric and symmetric C-C stretching mode. As for the bands of medium intensity at 1382 , 1296 and 1248 cm^{-1} are assigned to asymmetric C-N stretching ($\nu_{as}(C-N)$) and the band at 1161 cm^{-1} has been attributed to symmetric C-N stretching ($\nu_s(C-N)$). The bands located at 1577 , 1463 and 1422 cm^{-1} are assigned to asymmetric and symmetric CNH and OH deformation vibration. The bands appeared between 913 and 500 cm^{-1} are attributed to CCN groups deformation vibrations. According to the previous works of $[PbCl_4]^{2-}$ anions, the internal vibrational modes of Pb-Cl appear below 400 cm^{-1} in IR spectrum [31].

3.5 Raman spectroscopy of $[C_6H_{16}N_2O]PbCl_4$

The Raman spectrum, presented in Fig. 8, show a strong band located at 150 cm^{-1} with two shoulders at 130 and 175 cm^{-1} and two other peaks at 58 and 84 cm^{-1} . According to previous studies and by comparison with the Raman spectrum of similar crystals in the low frequencies range [31–33], the first band is probably assigned to stretching vibrational modes of the Pb–Cl bonds. In fact, several peaks in the Raman spectra of other compounds crystals or bulks are observed between 50 and 200 cm^{-1} . The two remaining peaks are assigned to translational and vibrational modes of both the organic and the inorganic moieties.

3.6 Optic study

UV absorption of $[C_6H_{16}N_2O]PbCl_4$

As a consequence of the structural diversity, dimensional variability in the anion structures is also observed, and thus the dependence of electronic and optical properties on the dimensionality of the inorganic structural component can be studied. In particular, the iodide compounds $(R-NH_3)_2PbI_4$ have been most intensively investigated, mainly because they exhibit excitonic emission in the green–yellow spectral range and because of their easy thin film processing [34]. The solid state UV-vis spectrum of crystalline $C_6H_{16}N_2OPbCl_4$ was recorded at room temperature (Fig. 9). It showed two distinct absorption peaks at 250 and 290 nm, which is similar to results found in other studies treating MX₄-hybrid compounds [35–38]. The lowest energy absorption peak at 290 nm (4.27 eV) is due to band gap absorption and it corresponds to the excitation of free electron–hole pairs within the $[PbCl_4]^{2-}$ inorganic chains. This peak is due mainly to the absorption between Cl (5p) and Pb (6s) (band to band), in fact an electron is excited from the valence band (VB) to a permit level in the gap leaving a hole in the (VB) [39]. The band with maximum at 250 nm (4.96 eV) can be attributed to the absorption of a highest energetic level in the conduction band.

Photoluminescenc of $[C_6H_{16}N_2O]PbCl_4$

Fig. 10 shows the emission spectrum of the title compound. Previous work on the various organic inorganic hybrid compounds has revealed that the strong luminescence arises from an exciton state [40]. The luminescence originates from electronic transitions within the inorganic portions. The peak exhibits at 529 nm is arising from exciton recombination within the inorganic portions [41]. Under excitation, an electron is excited from the valence band (VB) to the conduction band (CB), leaving a hole in the valence band. The electron transition back to the ground that is the recombination of the electron and hole yields an emission (Fig. S4).

3.7 XPS analysis

X-ray photoelectron spectroscopy (XPS) is a versatile surface analysis technique that can be used for compositional and chemical states analysis. Since X-rays are used for the incident beam in XPS, the XPS technique causes very little charging of samples and thus it is useful for both electrically conductive and non-conductive materials. The hybrid compound $C_6H_{16}N_2OPbCl_4$ was dried and characterized by XPS. The surface chemical composition is reported in Table S2. The main peaks are O1s, N1s, C1s, Cl2p and Pb4f, centered at 532.2, 401.8, 285.4, 197.1 and 137 eV, respectively (Fig.11a). In addition, the survey spectrum for this crystal exhibits an N1s peak (400eV) assigned to the $(C_6H_{16}N_2O)$ cation. Interestingly, the

high resolution N1s spectrum of the title compound (Fig. 11b) is fitted with two components centered at 399.6 eV and 401.8 eV. Whilst the latter is assigned to the quaternized form of the ligand $\text{H}_2\text{N}^+(\text{CH}_2)_2$, the former could be due to a free amine of the $\text{HN}(\text{CH}_2)_2$ type, resulting from a deprotonation of the quaternized ion. Indeed, energy of 399.6 eV is consistent with nitrogen in amines [42].

The oxidation states of Pb were further confirmed by examination of the binding energy position of the Pb4f doublet. The Pb4fXP spectrum in Fig. 11c presents two peaks at 137eV ($\text{Pb}4f_{7/2}$) and 143 eV($\text{Pb}4f_{5/2}$); the position of the main $\text{Pb}4f_{7/2}$ is in line with Pb in the oxidation state II. All these results confirm the valence sum calculations of this compound [43].

3.8 DSC analysis

In order to determine the thermal stability of $\text{C}_6\text{H}_{16}\text{N}_2\text{OPbCl}_4$, the differential scanning calorimetric was carried out with a heating rate of $5 \text{ K}\cdot\text{min}^{-1}$ between 300 and 550 K. The results are given in Fig.12. The curve shows that the title compound undertakes endothermic phenomena during heating. The peak appears at 522.4 K (onset at 517.9 K) corresponds to the melting point, with an enthalpy of $51.74 \text{ J}\cdot\text{g}^{-1}$.The temperature of the melting point was confirmed by independent measurement using a Kofler heating bank.

4. Conclusion

The synthesis, crystal structure, optical properties and thermal analysis of (2-hydroxyethyl)piperazine-1,4-dium tetrachloroplombate (II), organic-inorganic hybrid compound, have been described. Single crystal X-ray diffraction showed the formation of title compound consisting of polymeric 1-D endless inorganic chains. The different entities are held together via $\text{N-H}\cdots\text{Cl}$, $\text{O-H}\cdots\text{Cl}$ and $\text{C-H}\cdots\text{Cl}$ hydrogen bonds to build a three dimensional network. The Hirshfeld surface analysis reveals the percentage of intermolecular contacts of the title compound which shows that the $\text{H}\cdots\text{Cl}$ interactions represent the important percentage of the total surface and thus confirming the X-ray diffraction (XRD) results. The powder XRD was homogeneous with the single crystal. Moreover, the studies of optical and luminescence activities revealed that this compound exhibited two absorption bands and a strong emission at room temperature. DSC analysis showed that this compound is stable until the melting point. The XPS study confirmed the valence sum calculations of the $\text{C}_6\text{H}_{16}\text{N}_2\text{OPbCl}_4$.

Supplementary data

Crystallographic data for the structural analysis have been deposited on the Cambridge Crystallographic data Center (CCDC 1514267), and copies of the data can be obtained free of charge at www.ccdc.cam.ac.uk/conts/retrieving.html. Additional experimental details, structural characterization data (Projection along the *a*-axis showing the polymeric and 1-D endless inorganic chain, projection of the structure of $[\text{C}_6\text{H}_{16}\text{N}_2\text{O}]^{2+}$ cation along the *a*-axis showing the chair conformation of piperazinium entities, contributions to the Hirshfeld surface area for $\text{C}_6\text{H}_{16}\text{N}_2\text{OPbCl}_4$ and model for the formation and recombination of the exciton in the title compound are given in Fig S1-S4 and selected bond distances and angles in $[\text{C}_6\text{H}_{16}\text{N}_2\text{O}]\text{PbCl}_4$ and surface composition (in atomic %) are given in Table S1 and S2.).

Acknowledgments

Financial support from Spanish MINECO (MAT2016-78155-C2-1-R, MAT2013-40950-R, and FPI grant BES-2011-046948 to MSM.A.), *Gobierno del Principado de Asturias* (GRUPIN14-060), FEDER, and the Secretary of State for Scientific Research and Technology of Tunisia, are acknowledged.

References

- [1] D.G. Billing, A. Lemmerer, *Cryst. Eng. Comm.*, 8 (2006), 686-695.
- [2] X.H. Zhu, N. Mercier, P. Frere, P. Blanchard, J. Roncali, M. Allain, C. Pasquier, A. Riou, *Inorg. Chem.*, 42 (2003), 5330-5339
- [3] Aruta, F. Licci, A. Zappettini, F. Bolzoni, F. Rastelli, P. Ferro, T. Besagni, *Appl. Phys. A*, 81 (2005), 963–968.
- [4] K.N. Rao, A. Singh, G.V. Prakash, *Matter. Res. Bull.*, 52 (2014), 81-87.
- [5] C.R. Kagan, D.B. Mitzi, C. Dimitrakopoulos, *Science*, 286 (1999), 945-947.
- [6] D.B. Mitzi, *Chem. Mater.*, 8 (1996), 791-800.
- [7] X.H. Zhu, N. Mercier, M. Allain, P. Frere, P. Blanchard, J. Roncali, A. Riou, *J. Solid State Chem.*, 177 (2004), 1067–1071.
- [8] S. Zhang, G. Lanty, T.S. Lauret, E. Deleporte, P. Audebert, L. Galmiche, *Acta Mater.*, 57 (2009), 3301-3309.
- [9] G. Liu, J. Shi, X. Han, X. Zhang, K. Li, J. Li, T. Zhang, Q. S. Liu, Z. Zhang, C. C. Li, *Dalton Trans.*, 44 (2015), 12561-12575.
- [10] K. Tanaka, T. Takahashi, T. Kondo, K. Umeda, K. Ema, T. Umebayashi, K. Asai, K. Uchida, N. Miura, *J. Appl. Phys.*, 44 (2005), 5923-5932.
- [11] C. Aruta, F. Licci, A. Zappettini, F. Bolzoni, F. Rastelli, P. Ferro, T. Besagni, *Appl. Phys. A*, 81 (2005), 963–968.
- [12] H.H. Li, Z.R. Chen, L.C. Cheng, J.B. Liu, X.B. Chen, J.Q. Li, *Cryst. Growth. Des.*, 8 (2008), 4355-4358.
- [13] N. Mercier, N. Louvain, W. Bi, *Cryst. Eng. Comm.*, 11 (2009), 720–734.
- [14] M. Essid, M. Rzaigui, H. Marouani, *J. Chem. Crystallogr.*, 45 (2015), 310-317.
- [15] M.R. Shehata, M.M. Shoukry, S.A. Shokry, M.A. Mabrouk, *J. Coord. Chem.*, (2015), 3135-3147.
- [16] S. Soudani, E. Jeanneau, C. Jelsch, F. Lefebvre, C. Ben Nasr, *J. Mol. Struct.*, 1123 (2016), 66-74.
- [17] G. Liu, X. Zhang, H. Wang, H. Xu, Z. Wang, X. Meng, Y. Dong, R. Zhao, C. Li, *Dalton Trans.*, 46(2017), 12474-12486.
- [18] G. Liu, L. Liu, Y. Chu, Y. Sun, Z. Zhang, C. Li, *Eur. J. Inorg. Chem.*, 2015 (2015), 478-487.
- [19] Y. Liu, P. Yang, J. Meng, *Solide State Sciences*, 13 (2011) 1036-1040.
- [20] R.H. Blessing, *Acta. Crystallogr.*, A 51 (1995), 33-38.
- [21] G.M. Sheldrick, *Acta. Crystallogr.*, A 64 (2008), 112.

- [22] L.J. Farrugia, *J. Appl. Crystallogr.*, 32 (1999), 837-838.
- [23] K. Brandenburg, *DIAMOND Version 2.0*, 1998.
- [24] C.F. Macrae, P.R. Edgington, P. McCabe, E. Pidcock, G.P. Shields, R. Taylor, M. Towler, J. Van de Streek, *J. Appl. Crystallogr.*, 39 (2006), 453-457.
- [25] S.K. Wolff, D.J. Grimwood, J.J. McKinnon, M.J. Turner, D. Jayatilaka, M.A. Spackman, *2013 Crystal Explorer ver. 3.1*, University of Western Australia, Perth, 2012.
- [26] S. Soudani, V. Ferretti, C. Jelsch, F. Lefebvre, C. BenNasr. *J. Solid State Chem.*, 237 (2016), 7–13.
- [27] S. Wang, D.B. Mitzi, C.A. Field, A. Guloy, *J. Am. Chem. Soc.*, 117 (1995), 5297-5302.
- [28] D.E. Partin, M.J.O. Keeffe, *J. Solid State Chem.*, 95 (1991), 176–183.
- [29] D. Cremer, J.A. Pople, *J. Am. Chem. Soc.*, 97 (1975), 1354-1358.
- [30] S. BelhajSalah, P.S. Pereira da Silva, F. Lefebvre, C. Ben Nasr, S. Ammar, M.L. Mrad, *J. Mol. Struct.*, 1137 (2017) 553-561.
- [31] I. Baltog, M. Baibarac, S. Lefrant, *J. Phys. Condens. Matter.*, 21 (2009), 25507-25512.
- [32] J.F. Condeles, R.A. Ando, M. Mulato, *J. Mater. Sci.*, 43 (2008), 525–529.
- [33] N. Preda, L. Mihut, M. Baibarac, I. Baltog, R. Ramer, J. Pandele, C. Andronescu, V. Fruth, *J. Mater. Sci.: Mater. Electron.*, 20 (2009), 5465–5470.
- [34] A. Kessentini, M. Belhouchet, J.J. Sunol, Y. Abid, T. Mhiri, *J. Mol. Struct.*, 1039 (2013), 207-213.
- [35] A. Kessentini, M. Belhouchet, J.J. Sunol, Y. Abid, T. Mhiri, *J. Mol. Struct.*, 1039 (2013), 207.
- [36] A. Kessentini, M. Belhouchet, J.J. Sunol, Y. Abid, T. Mhiri, *J. Lumin.*, 149 (2014), 341.
- [37] T. Dammak, H. Boughzala, A. Mlayah, Y. Abid, *J. Lumin.*, 173 (2016), 213-217.
- [38] C. Hrizi, A. Samet, Y. Abid, S. Chaabouni, M. Fliyou, A. Koumina, *J. Mol. Struct.*, 992 (2011), 96-101.
- [39] M.S. Lassoued, M.S.M. Abdelbaky, A. Lassoued, R.M. Meroño, S. Ammar, A. Gadri, A. Ben Salah, S. García-Granda, *J. Mol. Struct.*, 1141 (2017), 660-667.
- [40] L.Q. Fan, L.M. Wu, L. Chen, *Inorg. Chem.*, 45 (2006), 3149-3151.
- [41] G.C. Papavassiliou, A.P. Patsis, D.J. Lagouvardos, I.B. Koutselas, *Synth. Met.*, 55 (1993), 3889-3894.
- [42] P.G. Antonov, Yu.N. Kukushkin, V.G. Shtrele, Yu.P. Kostikov, F.K. Egrov, *Zh. Neorg. Khimili.*, 27 (1982), 3130-3136.
- [43] G. Tan, D. Xiao, *Sep. Sci. Technol.*, 43 (2008), 2196-2207.

Figure captions

Fig. 1 Simulated and experimental XRD of $C_6H_{16}N_2OPbCl_4$.

Fig. 2 View of the asymmetric unit in the crystal structure of the title compound showing the atom-numbering scheme and displacement ellipsoids drawn at the 50% probability level.

Fig. 3 Projection along the *b*-axis of an inorganic layer. Hydrogen bonds are denoted by dotted lines. The organic entities are omitted for figure clarity.

Fig. 4 Projection along the *a*-axis showing the three dimensional network in the title compound. Hydrogen bonds are denoted by dotted lines.

Fig. 5 Hirshfeld surfaces mapped with d_{norm} , shape index and curvedness for $C_6H_{16}N_2OPbCl_4$.

Fig. 6 Fingerprint plots of all contacts in $C_6H_{16}N_2OPbCl_4$.

Fig. 7 Infrared absorption spectrum of $C_6H_{16}N_2OPbCl_4$.

Fig. 8 Raman spectrum of the title compound in the $[500-100] \text{ cm}^{-1}$ range.

Fig. 9 UV visible absorptionspectrum of $C_6H_{16}N_2OPbCl_4$.

Fig.10 Photoluminescence spectrum of $C_6H_{16}N_2OPbCl_4$.

Fig. 11 $C_6H_{16}N_2OPbCl_4$: **(a)** XPS survey scans, **(b)** N1s narrow region, and **(c)** high-resolution Pb4f.

Fig. 12 DSC thermogram of $C_6H_{16}N_2OPbCl_4$.

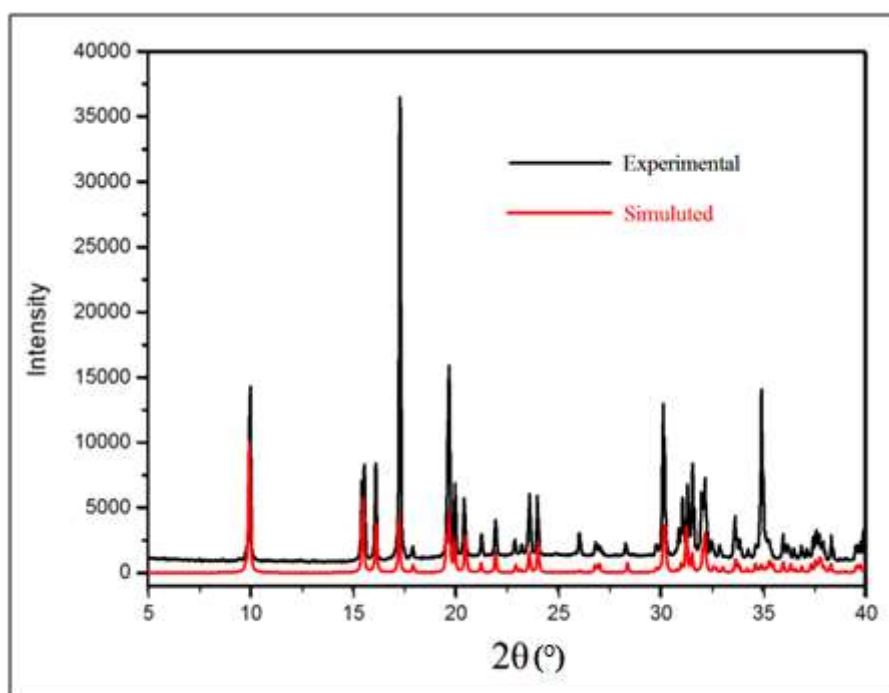


Fig. 1

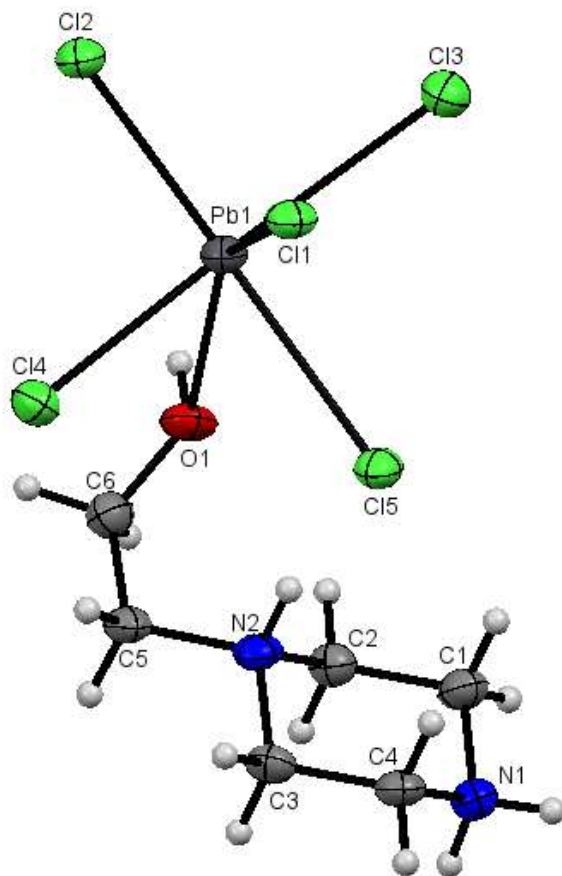


Fig. 2

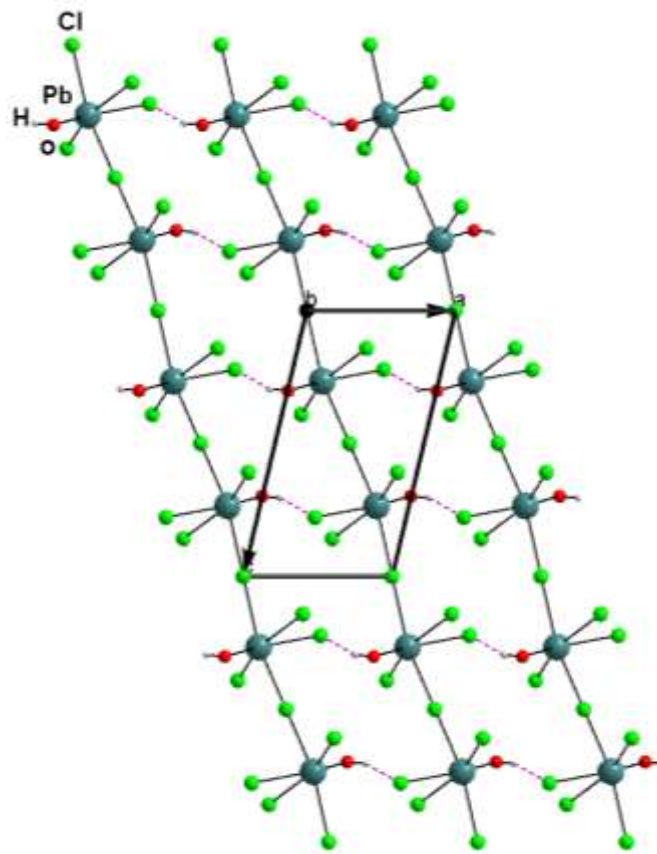


Fig.3

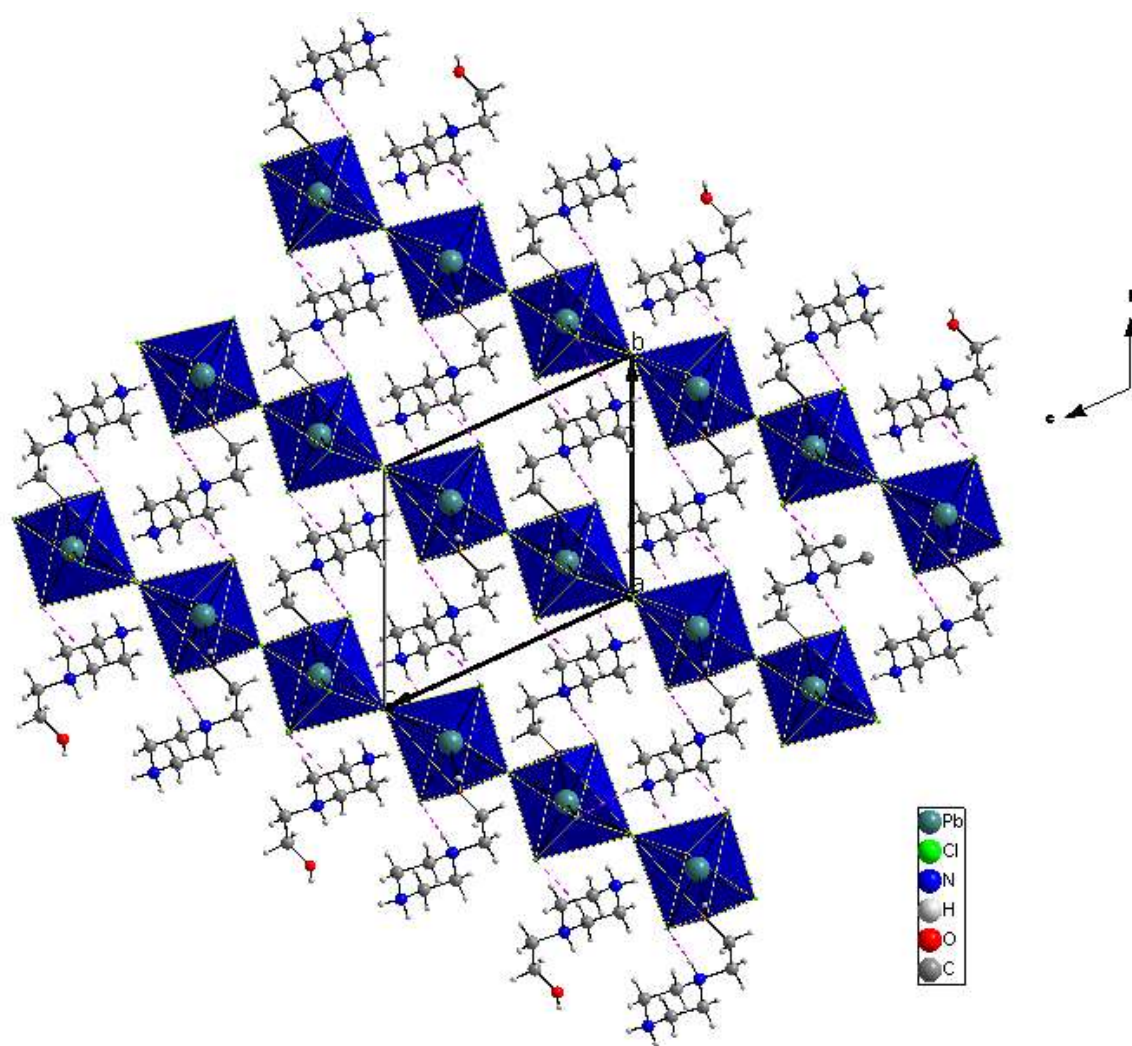


Fig. 4

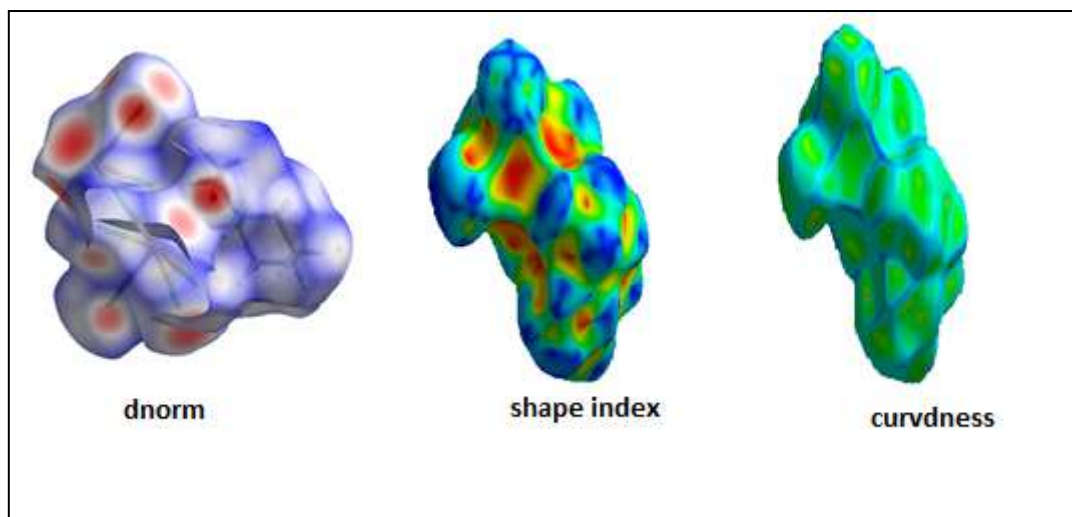


Fig.5

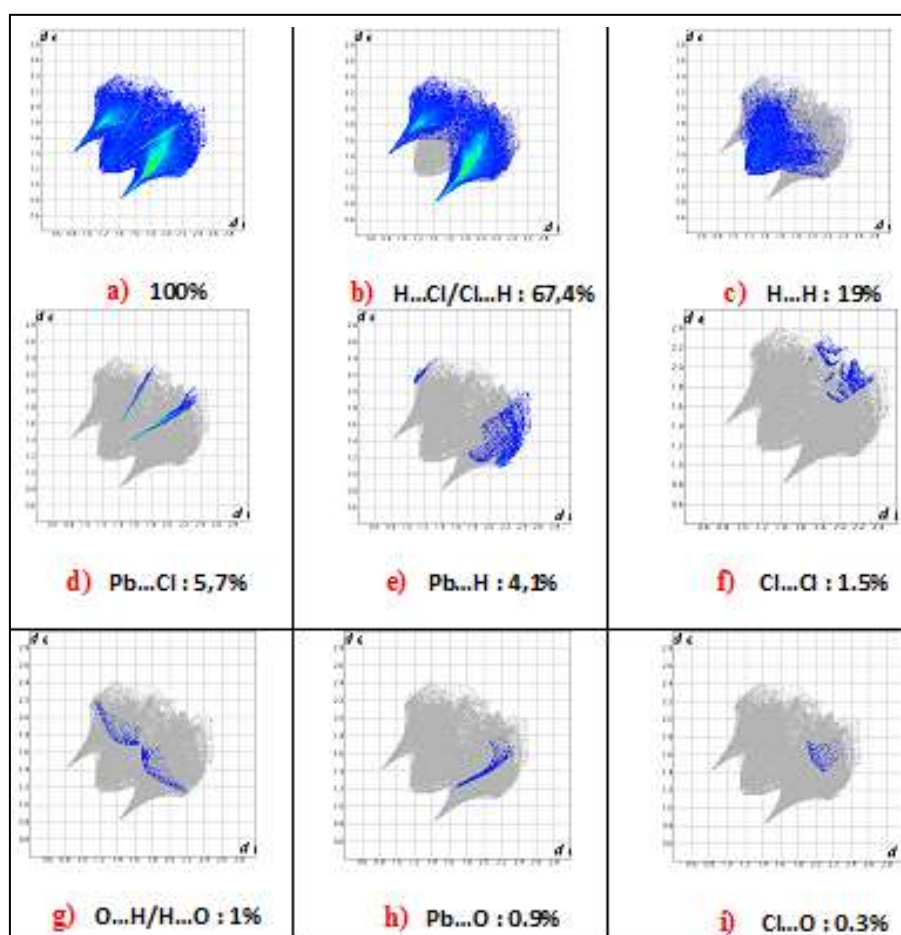


Fig. 6

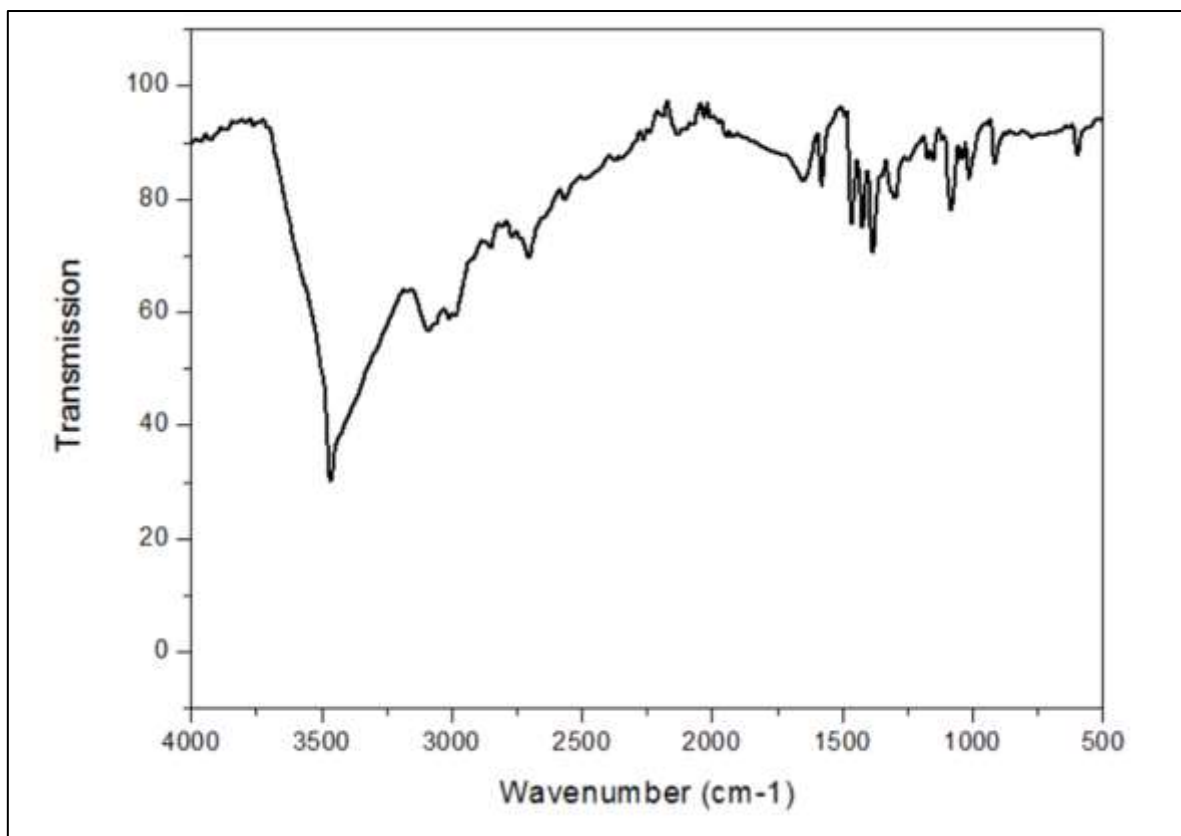


Fig. 7

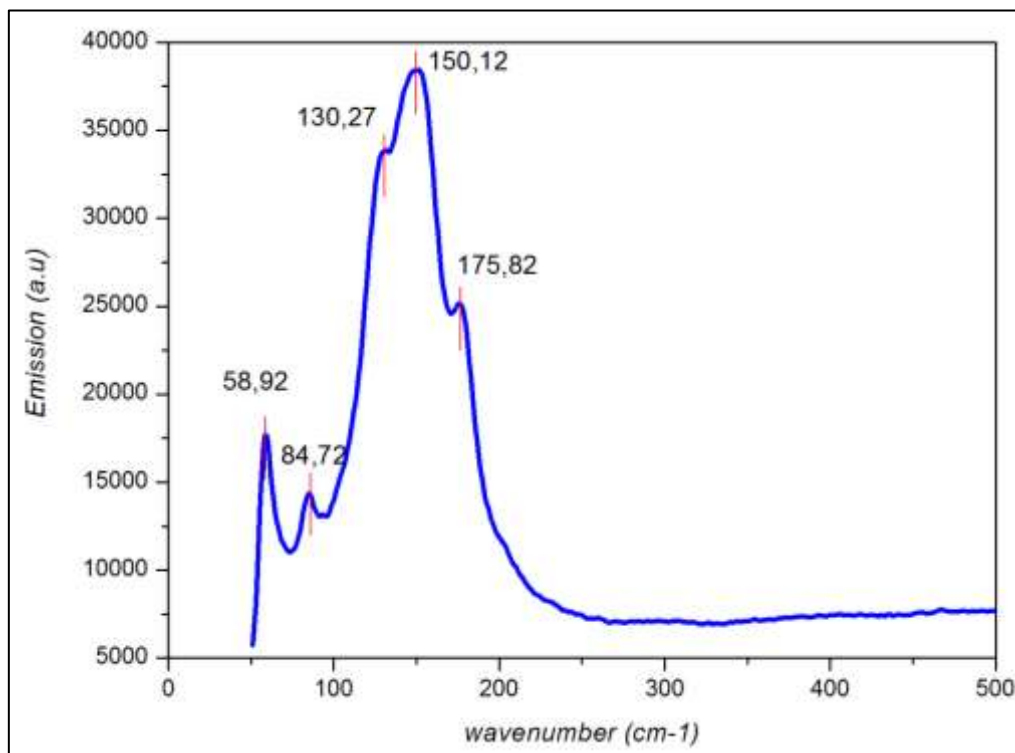


Fig.8

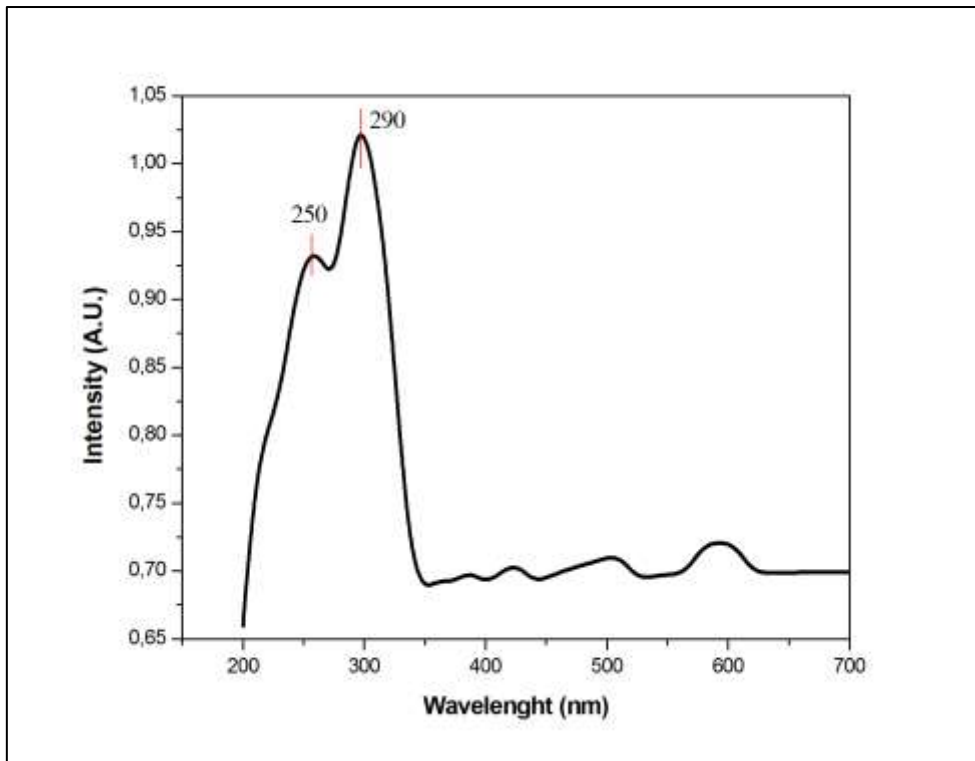


Fig.9

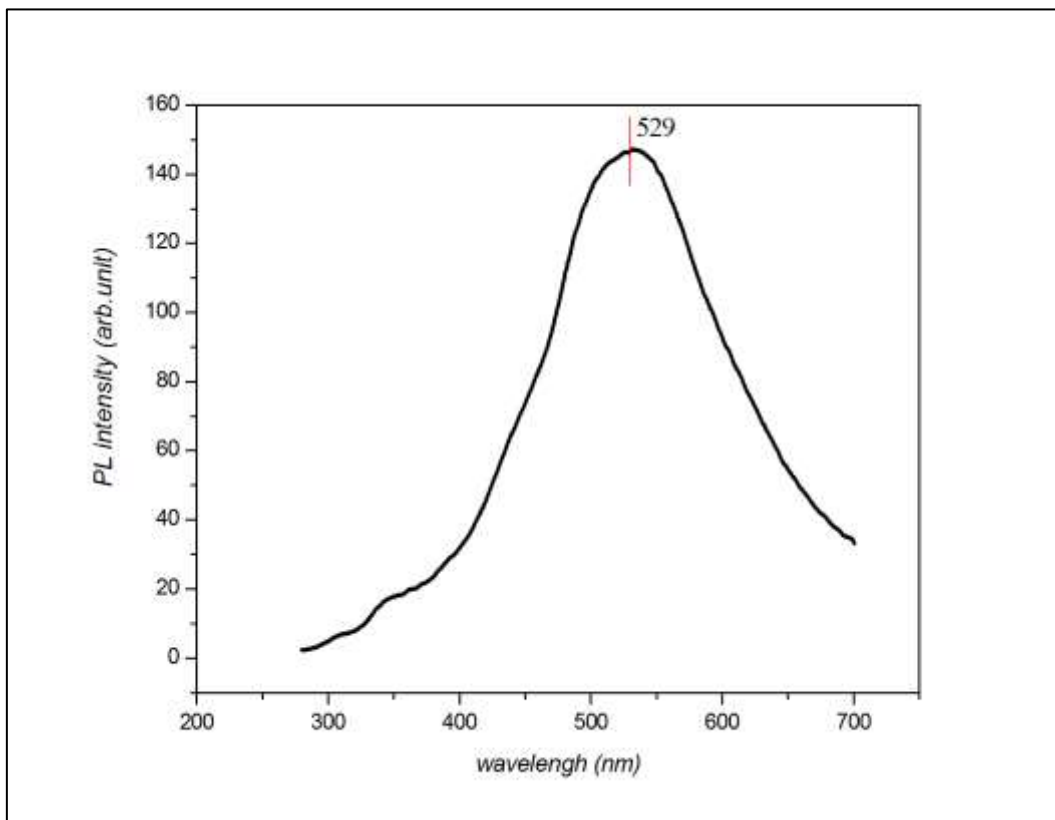


Fig. 10

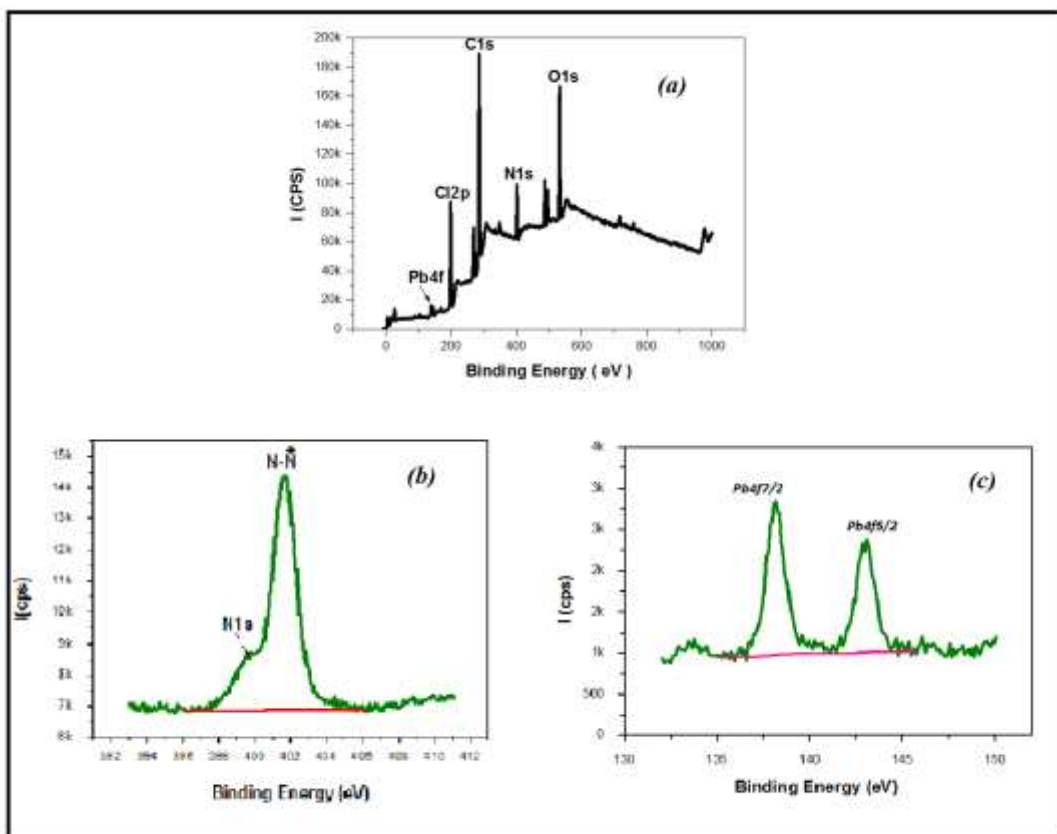


Fig.11

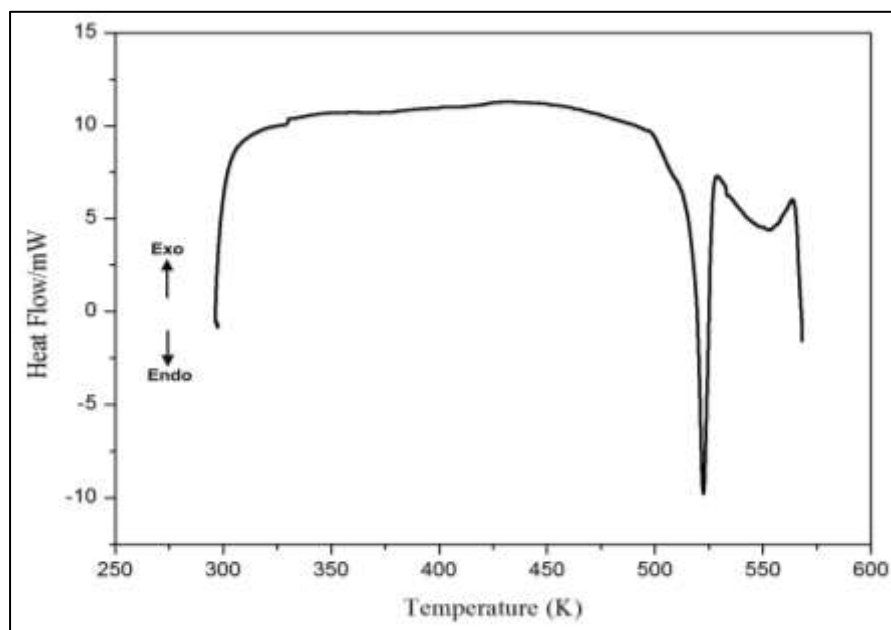


Fig.12

Table 1. Experimental details

Crystal data	
Chemical formula	C ₆ H ₁₆ N ₂ OPbCl ₄
M_r	481.20
Crystal system, space group	Triclinic, <i>P</i> -1
Temperature (K)	293
a, b, c (Å)	5.9926 (2), 10.3691 (5), 11.3558 (4)
α, β, γ (°)	111.755 (4), 96.080 (3), 105.948 (4)
V (Å ³)	612.85 (4)
Z	2
Radiation type	Mo $K\alpha$
μ (mm ⁻¹)	14.61
Crystal size (mm)	0.77 × 0.52 × 0.27 × 0.30 (radius)
Data collection	
Diffractometer	Xcalibur, Ruby, Gemini
T_{\min}, T_{\max}	0.005, 0.022
No. of measured, independent and observed [$I > 2\sigma(I)$] reflections	9084, 2160, 2150
R_{int}	0.067
$(\sin \theta/\lambda)_{\text{max}}$ (Å ⁻¹)	0.594
Refinement	
$R[F^2 > 2\sigma(F^2)], wR(F^2), S$	0.048, 0.125, 1.06
No. of reflections	2160
No. of parameters	131
$\Delta\rho_{\text{max}}, \Delta\rho_{\text{min}}$ (e Å ⁻³)	4.54, 2.02

Table 2. Hydrogen-bond geometry (Å, °)

D—H···A	D—H	H···A	D···A	D—H···A
N2—H2···Cl5	0.91	2.25	3.145 (10)	167
C2—H2B···Cl2 ⁱ	0.97	2.63	3.541 (12)	156
N1—H1A···Cl1 ⁱⁱ	0.91	2.44	3.270 (9)	154
N1—H1B···Cl1 ⁱ	0.91	2.52	3.244 (10)	137
O1—H1···Cl1 ⁱⁱⁱ	0.82	2.40	3.156 (9)	154

Symmetrycodes: (i) $x, y-1, z$; (ii) $-x+1, -y+1, -z+2$; (iii) $x+1, y, z$.